PTEP

Prog. Theor. Exp. Phys. **2022**, 04A103 (13 pages)
DOI: 10.1093/ptep/ptab105

Pb/Bi heterostructure as a versatile platform to realize topological superconductivity

Ikuko Watanabe[1], Seigo Souma[2,3], Kosuke Nakayama[1,4], Katsuaki Sugawara[1,2,3,4], Chi Xuan Trang[1], Kouji Segawa[5], Kunihiko Yamauchi[6,7], Tamio Oguchi[6,8], Takashi Takahashi[1,2,3], and Takafumi Sato[1,2,3,9,*]

[1]*Department of Physics, Faculty of Science, Tohoku University, Sendai 980-8578, Japan*
[2]*Center for Spintronics Research Network, Tohoku University, Sendai 980-8577, Japan*
[3]*Advanced Institute for Materials Research (WPI-AIMR), Tohoku University, Sendai 980-8577, Japan*
[4]*Precursory Research for Embryonic Science and Technology (PRESTO), Japan Science and Technology Agency (JST), Tokyo, 102-0076, Japan*
[5]*Department of Physics, Kyoto Sangyo University, Kyoto 603-8555, Japan*
[6]*Institute of Scientific and Industrial Research, Osaka University, Ibaraki, Osaka 567-0047, Japan*
[7]*Center for the Promotion of Interdisciplinary Education and Research (CPIER), Kyoto University, Kyoto 606-8317, Japan*
[8]*Center for Spintronics Research Network, Osaka University, Toyonaka, Osaka 560-8531, Japan*
[9]*International Center for Synchrotron Radiation Innovation Smart (SRIS), Tohoku University, Sendai 980-8577, Japan*
*E-mail: t-sato@arpes.phys.tohoku.ac.jp

Received July 6, 2021; Revised August 5, 2021; Accepted August 6, 2021; Published September 4, 2021

Realization of topological superconductors (TSCs) hosting Majorana fermions is an exciting challenge in materials science. Majorana fermions are predicted to emerge at vortex cores of two-dimensional (2D) TSCs and at both ends of one-dimensional (1D) TSCs; these two types of TSCs have been explored independently in different materials. Here, a system which has a potential to access both 1D and 2D TSCs in a single platform, Pb(111)/Bi(111) heterostructure, is proposed. One to twenty bilayers (BLs) of Bi(111) ultra-thin films are epitaxially fabricated on $TlBiSe_2$, and an intriguing evolution of electronic states upon variation of Bi-layer thickness is revealed by angle-resolved photoemission spectroscopy. The metallic quantum-well states at 1–2BLs are found to turn into the Rashba states at 5–20BLs, via the semiconducting states at 3BL. Fabrication of a Pb(111) film on 20BL Bi(111) enables observation of the proximity-induced superconductivity in Bi(111) as evident from a 1 meV energy gap at 5 K; these energy and temperature scales are considerably larger than those of Rashba superconductors. The Pb/Bi heterostructure serves as a versatile platform to study the interplay among proximity-induced superconductivity, band structure, and topology.

Subject Index I40, I60, I90

1. Introduction

A topological insulator (TI) is an exotic quantum state characterized by an insulating bulk-band gap and a metallic surface/edge state protected by time-reversal symmetry associated with non-trivial topology of wave functions originating from the strong spin–orbit coupling (SOC) [1–3]. Discovery of TIs initiated the search for even more exotic symmetry-protected topological phases, as represented by topological semimetals protected by specific crystal symmetries and topological superconductors (TSCs) with time-reversal-invariant or chiral characteristics. TSCs are a superconducting (SC) analogue of TI wherein an SC gap, instead of the band gap, accompanies gapless boundary states

often consisting of Majorana fermions [2,4,5]. Due to the particle–antiparticle symmetry and non-Abelian-statistics nature, Majorana fermions are thought to be applicable to fault-tolerant quantum computations [6–9]. While the boundary states of three-dimensional (3D) TSCs appear at the surface as a helical Majorana cone displaying a Dirac-type energy dispersion, Majorana fermions useful for quantum computations appear in the time-reversal-symmetry broken state as the Majorana zero mode in the vortex core of two-dimensional (2D) TSCs as well as at both ends of one-dimensional (1D) TSCs [7,10–13]. Thus, the major interest of current research is to find 2D and 1D TSCs hosting robust Majorana fermions.

To realize such TSCs, various superconducting hybrids involving materials with strong SOC have been intensively investigated, as initiated by the theoretical prediction of topological superconductivity in effectively *p*-wave superconducting states of helical Dirac fermions and Rashba states [10,13]. Such hybrids involve Bi_2Se_3, Bi_2Te_3, HgTe, and Bi(111) ultra-thin films grown on a conventional superconductor [14–20] (for 2D TSC), InSb/InAs nanowires in contact with a conventional superconductor [21–23], and an Fe atomic chain on Pb [24] (for 1D TSC), etc. Surfaces of doped superconducting TIs [25,26] and iron-based superconductors [27,28] are another group of candidates for a 2D-TSC platform. As highlighted by these examples, material exploration of TSC candidates is rapidly in progress, whereas such investigations have hitherto been performed almost independently between 1D and 2D cases. To discuss a unified picture regarding superconductivity, dimensionality, and topology, it may be useful to search for a single experimental platform which can access both 1D and 2D TSCs.

We have chosen a Bi(111) ultra-thin film as a potentially useful material to address the above issue by considering the strong SOC and the quantum confinement effect. The 2D Rashba surface state (SS) in a thick regime [29] and the 1D edge state in the quantum-spin-Hall (QSH) insulator phase predicted for the one bilayer (1 BL) regime [30] may be useful for realization of 2D and 1D TSCs [Fig. 1(a)], respectively. However, one needs to overcome two major experimental difficulties: (i) the thickness (d) of the Bi(111) film must be systematically controlled down to a 1 BL limit, and (ii) superconductivity at reasonably high temperature must be induced in the film. It is noted that bulk Bi crystal shows superconductivity at ultralow temperature below 0.53 mK [31], but this temperature is obviously insufficient for feasible measurements and applications.

In this paper we have epitaxially grown Bi(111) films with various thickness on top of a three-dimensional (3D) topological insulator (TI) $TlBiSe_2$ (called here TBS) taking into account the good lattice matching [32], and have further fabricated a heterostructure involving an epitaxial Pb(111) film on Bi(111) [see Fig. 1(b)] using the molecular-beam epitaxy (MBE) method specialized for Pb-film growth. By utilizing in situ angle-resolved photoemission spectroscopy (ARPES), we have clarified the evolution of electronic states as a function of thickness for Bi(111)/TBS. We have further succeeded in inducing proximity-induced superconductivity in the Bi(111) film, as evidenced by the opening of an energy gap below T_c of the Pb film. We discuss the implication of the present results in relation to dimensionality, and Rashba and topological superconductivity.

2. Experiments

High-quality single crystals of TBS were grown by a modified Bridgman method [33]. To prepare a Bi(111) film, we first cleaved a TBS crystal under ultra-high vacuum with scotch tape to obtain a shiny mirror-like surface, and then deposited Bi atoms on the TBS substrate using the MBE technique while keeping the substrate temperature at 300 K. To fabricate a Pb(111)/Bi(111) heterostructure, we further deposited Pb atoms on Bi(111)/TBS, keeping the substrate temperature at $T = 85$ K. The film

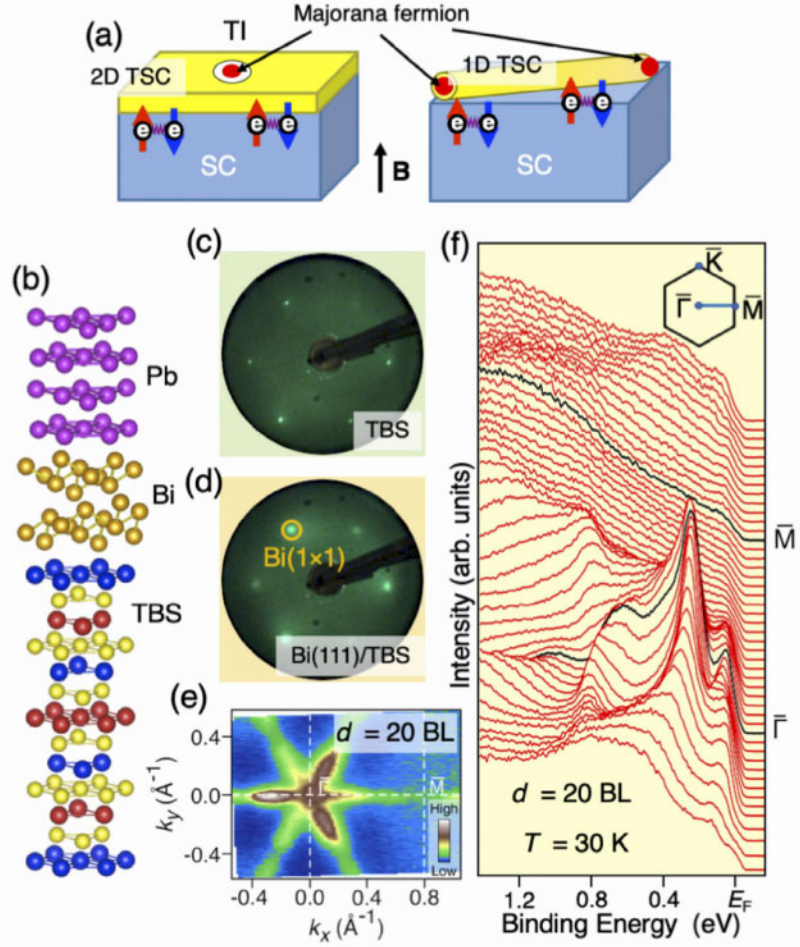

Fig. 1. (a) Schematic view of 2D and 1D topological superconductivity accompanying the Majorana zero mode in hybrids involving an *s*-wave superconductor. (b) Heterostructure consisting of Pb(111), Bi(111), and TBS. (c, d) LEED patterns of (c) cleaved TBS and (d) 20BL-Bi(111)/TBS, respectively, measured at room temperature with a primary electron energy of 100 eV. (e) ARPES intensity mapping at E_F measured at $T = 30$ K with He-Iα photons ($h\nu = 21.218$ eV). (f) EDCs for 20BL-Bi(111)/TBS measured along the $\bar{\Gamma}\bar{M}$ cut in the surface BZ of TBS.

thickness was controlled by the deposition time at a constant deposition rate. The crystallinity and lattice constants of the samples were characterized by the LEED measurement. ARPES measurements were performed with the MBS-A1 and SES-2002 electron analyzers equipped with a high-intensity He discharge lamp. After the growth of Pb/Bi heterostructure by evaporation at liquid N_2 temperature in the MBE chamber, the film was immediately transferred to the sample cryostat kept at $T = 30$ K in the ARPES chamber, to avoid the clusterization of Pb which is accelerated at room temperature [34]. The clusterization of Pb prevented us from removing samples from the MBE-ARPES chamber while keeping the crystallinity of the Pb film to perform ex situ experiments such as transmission electron microscopy and electrical transport measurements. We used the He-Iα resonance line ($h\nu = 21.218$ eV) to excite photoelectrons. The energy resolution of ARPES measurements was set to be 2–40 meV. The sample temperature was kept at $T = 30$ K during the ARPES-intensity-mapping measurements, while $T = 5$ and 10 K for the SC-gap measurements. The E_F of the samples was referenced to that of a gold film electrically in contact with the sample holder.

3. Results and discussion

First we present the characterization of Bi(111) thin film on TBS. Figure 1(c) shows the low-energy electron diffraction (LEED) pattern of a cleaved surface of TBS. The appearance of clear 1×1 spots suggests a well-ordered surface. When depositing 20 BL Bi(111) on TBS [Fig. 1(d)], the LEED pattern exhibits a 1×1 periodicity similar to that of TBS. In fact, the location of spots nearly coincides with that of TBS, showing good lattice matching [32]. The ARPES intensity mapping at the Fermi level (E_F) for this film shown in Fig. 1(e) reveals a pronounced intensity from six elongated pockets (hole pockets) that surround a small circular pocket (electron pocket) at the $\bar{\Gamma}$ point in the Brillouin zone (BZ), similarly to the case of Bi(111) films on other substrates [35–38]. These hole and electron pockets originate from the SSs with Rashba spin splitting, whose metallic nature is confirmed by a clear Fermi-edge cut-off in the energy distribution curves (EDCs) around the $\bar{\Gamma}$ point [Fig. 1(f)].

Now that good single crystallinity is established for thick films, next we present the evolution of electronic states down to the 1 BL limit. It is emphasized that 1 BL Bi(111) film can hardly be fabricated on other substrates such as Si(111), graphene, and TaS_2 [35,37,38] due to the (111)-to-(110) structural phase transition. The Fermi surface (FS) mappings around the $\bar{\Gamma}$ point in Fig. 2(a) and corresponding ARPES intensity plots along the $\bar{\Gamma}\bar{K}$ cut in Fig. 2(b) signify a similar intensity profile between $d = 20$ and 5 BL, in particular for the presence of six lobes in the FS mapping [the **k** region of the FS mapping in the BZ is indicated by a gray shade in Fig. 2(c)]. This suggests that the Rashba SS survives down to $d = 5$ BL (note that the energy bands in the vicinity of E_F for $d = 5$ BL appears to show a small upward energy shift relative to those for $d = 20$ BL; this is likely associated with the charge transfer from the TBS substrate, as detailed later). On the other hand, one can recognize in $d = 1$ BL a marked difference in the intensity profile due to the difference in the FS topology; there exist a large snowflake-like hole pocket and a small circular hole pocket [each further splits into two pockets by the Rashba SOC, although they are not very visible in the current

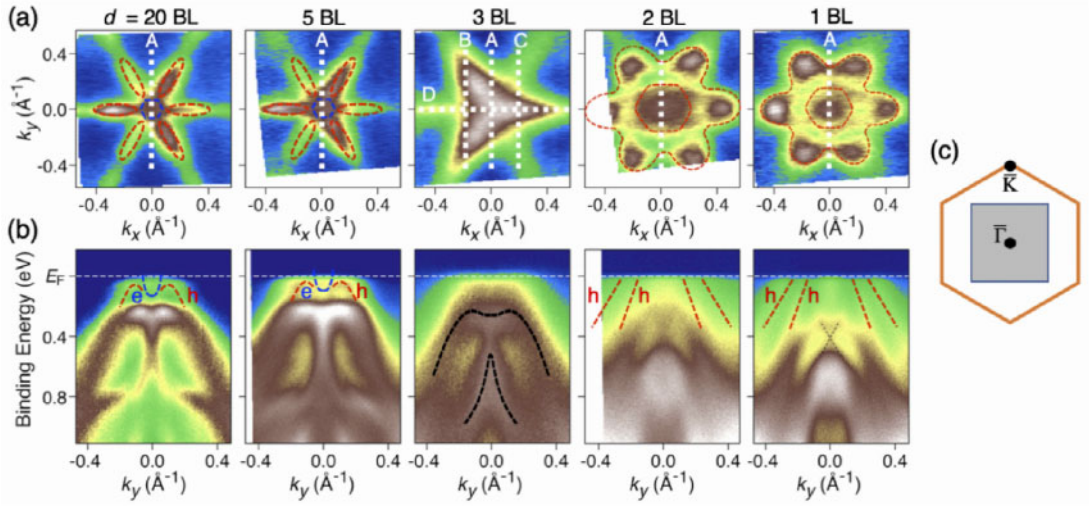

Fig. 2. (a) FS mapping and (b) ARPES intensity plot along the $\bar{\Gamma}\bar{K}$ cut [indicated as cut A in (a)] for Bi(111) films with various thicknesses ($d = 20$, 5, 3, 2, and 1 BL). The dashed lines for $d = 1$ BL in (b) highlight the Kramer's degeneracy associated with the hybridization of Bi- and TBS-derived bands due to the topological proximity effect [32]. (c) Surface BZ of Bi(111) and the **k** region (gray shade) where the FS mapping in (a) was performed.

(E, **k**) mesh]. They are quantum well states (QWSs) originating from the 2D bulk bands [32]. Similar metallic QWSs are also observed in $d = 2$ BL [Figs. 2(a) and 2(b)]. Here we briefly comment on the influence of the TI nature of the TBS substrate to the electronic states of Bi(111). It has been reported that the Dirac cone state migrates from the surface of TBS to 1 BL Bi(111) in the heterostructure due to the topological proximity effect [32], leading to the emergence of characteristic X-shaped dispersion at the binding energy E_B of $\sim$0.4 eV, as indicated by dashed black lines for $d = 1$ BL in Fig. 2(b). On the other hand, the migrating Dirac cone band is hard to resolve for $d = 2$ BL and completely absent for $d = 3$ BL [Fig. 2(b)], indicating that the characteristic length scale of the topological proximity effect is at most 1–2 BL. Thus, the TI nature of the substrate does not affect the electronic states of Bi(111) films thicker than 2 BL.

We found that the spectral feature for $d = 3$ BL is markedly different from the others. As seen in the middle panel of Fig. 2(b), no obvious E_F-crossing of bands is observed, unlike the metallic QWSs and Rashba SS in $d = 1$–2 and 5–20 BL, respectively. The tail of the topmost valence band forms a triangular intensity pattern at E_F [middle panel of Fig. 2(a)] instead of the six lobes (for $d = 5$, 20 BL) or the snowflake/circle (for $d = 1$, 2 BL). This suggests a peculiar characteristic of $d = 3$ BL (note that the intensity profile for $d = 4$ BL is similar to that for 3 BL; see Fig. A.1 of Appendix A). We have carefully measured the band dispersion around the valence-band top along several **k** cuts [cuts B–D in the middle panel of Fig. 2(a)] and always observed the absence of band crossing of E_F as shown in Figs. 3(a)–(c), indicating the semiconducting-like nature of $d = 3$ BL (note that we also found no Fermi surface around the M point; cut D in Fig. 3(c) includes the M point, $k_x \sim 0.8$ Å^{-1}) in contrast to the metallic behavior of both thinner and thicker films. It is noted that a previous ARPES study of Bi(111)/Bi_2Te_3 [36] reported qualitatively similar evolution of the ARPES intensity map as a function of d, whereas the conclusion regarding the insulating or metallic nature of the 3 BL film appears to be different, probably because of the difference in the substrate TIs and resultant differences in the lattice strain effect, interface condition, amount of charge transfer across the interface, etc.

How can we explain such characteristic thickness dependence of the band structure? To address this question, one needs to consider simultaneously (i) the quantum confinement effect and (ii) the charge transfer from the TBS substrate. As shown in Fig. 3(d), which displays a schematic band dispersion along the $\bar{\Gamma}\bar{K}$ cut obtained by the present experimental results and the band calculations for free-standing Bi(111) slabs [39], 1 BL Bi(111) has a large inverted band gap and likely hosts the QSH phase accompanying a gapless helical edge state [30,40]. However, due to the charge (electron) transfer from Bi to TBS [Fig. 3(e)] associated with the difference in the work function [Fig. 3(f)], the 1 BL Bi(111) film on TBS is actually hole-doped and the chemical potential is located below the valence band top. Thus, strictly speaking, the 1 BL Bi(111) on TBS is not a QSH "insulator." When d is increased, the inverted band gap is gradually decreased due to the quantum size effect [35] [3 BL case in Fig. 3(d)]. Eventually, the band inversion vanishes and the system transforms into a bulk metal accompanying the Rashba SS ($d = 5$–20 BL case in Fig. 3(d); note that only the SS is shown for simplicity). It is inferred that the $d = 3$ BL still keeps a finite inverted band gap, because of an expected smooth evolution of the band gap from the 1 BL side and the observed semiconducting-like electronic states at $d = 3$ BL [39]. Although the 1 BL film is unable to maintain the insulating state due to the excess hole doping from the TBS substrate, such a charge transfer effect becomes mild for $d = 3$ BL because the doped holes are widely distributed throughout the film and, consequently, the number of doped holes per unit BL decreases with increasing d, so that the chemical potential moves into the band gap (but still close to the valence band top) for $d = 3$ BL. We thus suggest that,

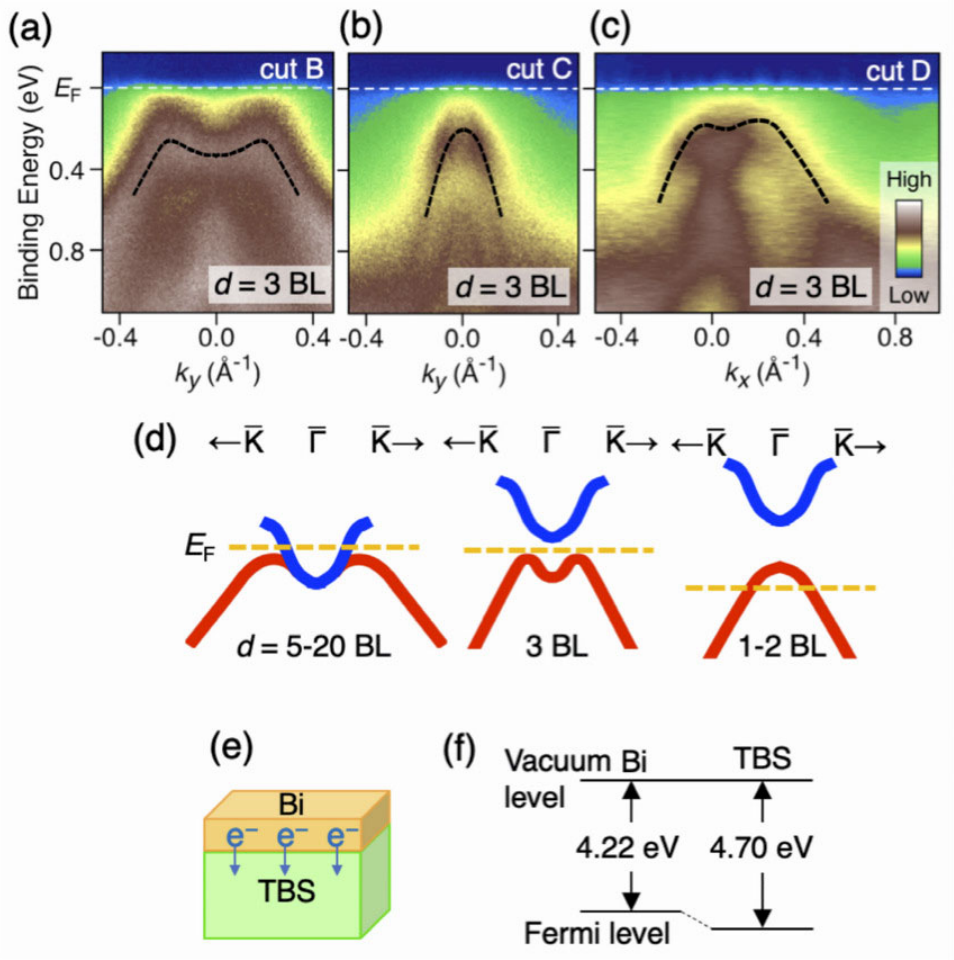

Fig. 3. (a)–(c) ARPES intensity plots measured along cuts (a) B, (b) C, and (c) D in the $d = 3$ BL data of Fig. 2(a). (d) Schematics of the evolution of the near-E_F band structure as a function of d in Bi(111)/TBS. (e,f) Schematics of the electron charge transfer from Bi(111) to TBS, and work functions of Bi and TBS relative to the vacuum level, respectively.

at the peculiar thickness of 3 BL, the quantum size effect and the charge transfer work cooperatively to realize a possible QSH insulator phase, although this conjecture needs to be further tested by directly observing the helical edge states using scanning tunneling microscopy (STM) and also by observing the quantized edge conduction in the electrical transport measurements. It is noted that in the transport measurements, we need to reduce the interference from the metallic TBS substrate.

Next, we address another important question: whether one can induce superconductivity on the Bi(111) film. For this, we deposited Pb atoms on the $d = 20$ BL film to fabricate a Pb/Bi heterostructure. The $d = 20$ BL film is well suited to clarifying the proximity-induced energy gap due to the high metallicity as inferred from the ARPES results in Figs. 1(e) and 1(f). The LEED pattern for the Pb film on Bi(111) in the inset to Fig. 4(a) signifies 1×1 spots (indicated by purple circles and the dashed purple hexagon) which are expanded by 30% relative to those of pristine 20 BL Bi(111) [yellow dashed hexagon, reproduced from Fig. 1(d)]. We have estimated the in-plane lattice constant of the Pb film to be 3.49 Å, which is close to that of bulk (3.50 Å) [41]. These results indicate that a Pb(111) single crystalline film is successfully grown on Bi(111), allowing us to investigate the electronic states of this hybrid film in detail. Figures 4(a)–(e) display the evolution of ARPES intensity

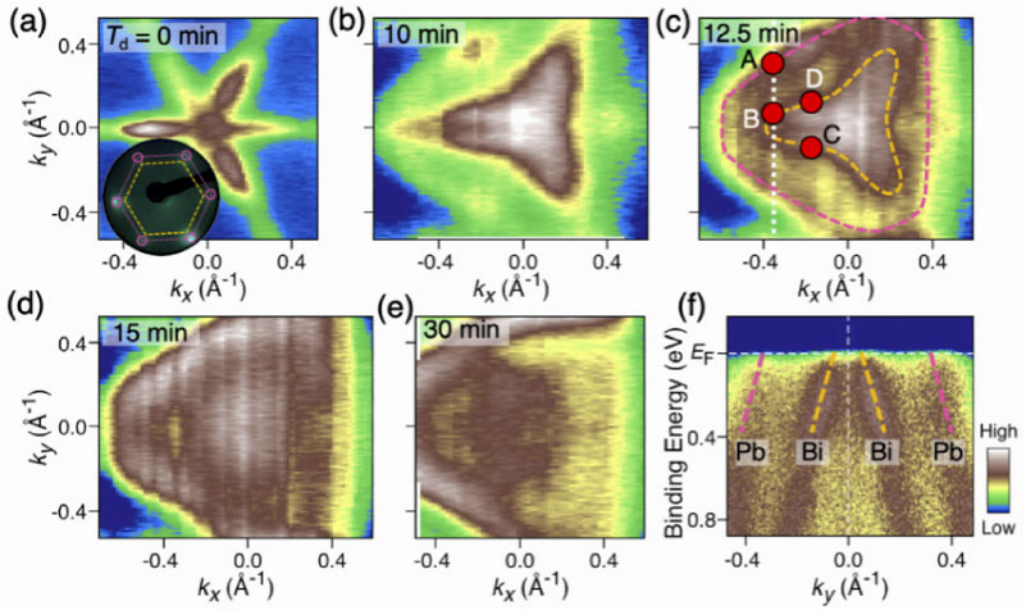

Fig. 4. (a)–(e) Evolution of ARPES intensity mapping at E_F for Pb(111)/20BL-Bi(111)/TBS as a function of Pb deposition time of (a) 0 min, (b) 10 min, (c) 12.5 min, (d) 15 min, and (e) 30 min. The inset to (a) shows a LEED pattern of Pb(111)/20BL-Bi(111) ($T_d = 15$ min) heterostructure measured at $T = 80$ K with a primary electron energy of 100 eV. The purple open circles and dashed hexagon are a guide for the eyes to highlight the spot. The location of 1×1 spots for Bi(111) [reproduced from Fig. 1(d)] is shown by a yellow hexagon to highlight the lattice mismatch. (f) ARPES intensity along the white dashed line in (c), measured at $T = 30$ K. The dashed lines trace the energy bands originating from Pb and Bi.

as a function of Pb deposition time (T_d). The six lobes seen for pristine 20 BL Bi(111) ($T_d = 0$ min) in Fig. 4(a) become fatter and more triangular for $T_d = 10$ min in Fig. 4(b). This is caused by finite hole doping to the Bi(111) from deposited Pb atoms due to the slightly larger work function of Pb than that of Bi [42]. On further depositing Pb, another large triangular intensity pattern starts to emerge outside the Bi-derived one [Fig. 4(c)]. This large FS is assigned to the Pb-derived FS [34] because its intensity is systematically increased upon Pb deposition and at the same time the inner Bi-derived pocket is gradually suppressed.

To experimentally establish the SC proximity effect in the Pb/Bi hybrid, it is essential to simultaneously demonstrate the SC nature of the Pb film and the proximity-induced superconductivity in the Bi film. For this purpose, we have chosen a sample with $T_d = 12.5$ min (the thickness of this Pb film was estimated to be ∼5 ML from the deposition rate), because we can resolve both Pb- and Bi-derived bands simultaneously [Figs. 4(c) and 4(f)] in this sample when we measure along a **k** cut crossing both pockets [white dashed line in Fig. 4(c)]. Figure 5(a) shows ultra-high-resolution EDCs at the Fermi wave vector (k_F) point of the Pb-derived FS [point A in Fig. 4(c)] measured at $T = 5$ and 10 K across the SC transition temperature T_c of bulk Pb (7.2 K). At $T = 5$ K, one can recognize a leading-edge shift toward higher E_B together with a pile up of the spectral weight slightly away from E_F, a typical signature of an SC gap opening. The coherence peak vanishes at $T = 10$ K due to the gap closure, as better visualized in the symmetrized EDC [Fig. 5(b)], which is generated by adding the original EDC [Fig. 5(a)] and the reversed EDC with respect to E_F to cancel out the influence of the Fermi–Dirac distribution function [43]. We have estimated the SC gap size at $T = 5$ K to be 1.1 meV from the numerical fittings with the Dynes function [44]. This value is close to that of bulk Pb (∼1.2 meV) [45].

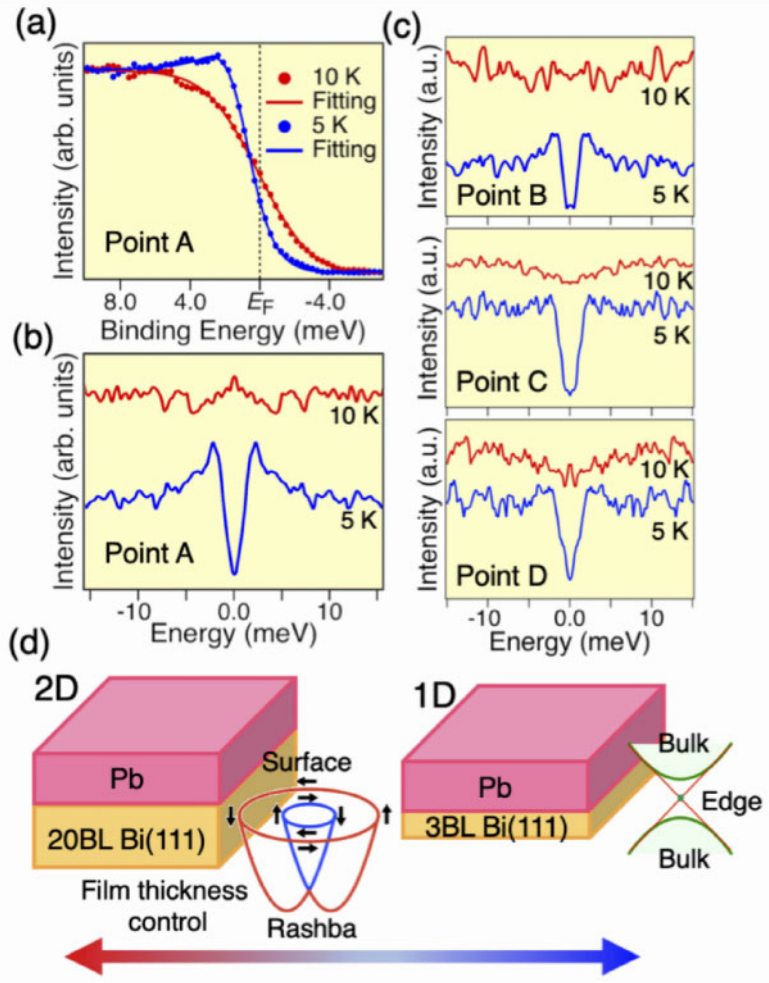

Fig. 5. (a) Ultra-high-resolution EDCs in the vicinity of E_F (filled circles) for $T_d = 12.5$ min, measured at $T = 10$ and 5 K (across T_c of Pb film) at point A (on the Pb-derived FS) in Fig. 4(c). The result of numerical fittings with the Dynes function [44] to the EDC at 5 K is shown by a solid curve. (b) EDCs symmetrized with respect to E_F at $T = 5$ and 10 K measured at point A in Fig. 4(c), highlighting the suppression of spectral weight around E_F at $T = 5$ K due to the SC gap opening. (c) As (b) but measured at points B–D in Fig. 4(c). (d) Schematics of the realization of possible 2D to 1D topological superconductivity through thickness control of Bi(111) film in contact with Pb.

Since the superconductivity is realized in the ultra-thin Pb film, we now address the essential question of whether the Bi(111) film exhibits proximity-induced superconductivity. We show in Fig. 5(c) the symmetrized EDC at $T = 5$ and 10 K measured at three representative k_F points on the Bi-derived FS [points B–D in Fig. 4(c)]. At point B, we observe a clear depletion of spectral weight at E_F indicative of a gap opening, while the gap completely vanishes at $T = 10$ K. The coherence peak seems less pronounced compared to that at point A, in accordance with the smaller gap size (0.9 meV). These observations strongly suggest that the proximity-induced superconductivity indeed shows up in the 20 BL Bi(111) film. We also found in Fig. 5(c) that a similar gap opens at points C and D closer to the $\bar{\Gamma}$ point. This suggests that an isotropic *s*-wave gap opens on the Bi-derived FS. It is noted that the magnitude of the proximity-induced gap of Bi ($\sim$0.9–1.1 meV) is comparable to the original gap of Pb ($\sim$1.2 meV). Since the proximity-induced gap is known to gradually decrease on moving away from the interface, we speculate that the observed gap originates mainly from the states

very close to the Pb/Bi interface. Such interface sensitivity may be reasonable because we detected photoelectrons from the interface through a thin Pb overlayer by utilizing a photoelectron escape depth slightly larger than the Pb overlayer thickness. We have also estimated the broadening factor Γ to be 0.5 and 0.8 meV at points A and B, respectively. These values are not so small compared to the gap magnitude of $\sim$1 meV, and almost comparable to the scale of thermal broadening (5 K $\sim$ 0.5 meV) at point A and larger at point B, in accordance with the observed large residual sub-gap density of states. This result suggests that disorder-induced in-gap broadening plays some role besides the thermal broadening, although it is difficult to distinguish each contribution due to the error bar originating from the experimental resolution and data statistics.

Observation of the proximity-induced superconductivity in Bi(111) has important implications for SC pairing. It is likely that proximity-induced superconductivity occurs on the spin-split Rashba SS (though it is hybridized with the bulk bands near E_F) caused by the inversion symmetry breaking at the interface and the strong SOC. This would not favor a simple singlet Cooper pairing, but would promote the mixing of singlet and triplet pairs, as generally discussed in noncentrosymmetric superconductors [46]. In this regard, the Pb(111)/Bi(111) heterostructure provides a useful platform to study the 2D Rashba superconducting state with a considerably higher T_c ($\sim$6–7 K) than those for other known Rashba or noncentrosymmetric 2D superconductors such as (Tl, Pb) ultrathin film on Si(111) ($T_c \sim 2.2$ K) [47] and monolayer 1H-$NbSe_2$ ($T_c \sim 1.5$ K) [48].

Now we discuss the possibility of 2D topological superconductivity. It has been suggested that the necessary conditions for realizing 2D TSC with the Rashba state are (i) to make a good heterointerface between a superconductor and a counterpart material that hosts Rashba states, (ii) to induce a pairing gap on the spin-split band, and (iii) to situate the Kramer's point of the Rashba state very close to E_F and then open up a Zeeman gap under a magnetic field while keeping the superconductivity. Conditions (i) and (ii) seem to be fulfilled in the present case. Condition (iii) is known as the Majorana condition, written as $\mu_B g H_z/2 > \sqrt{\Delta^2 + \mu^2}$ [13], where g, H_z, Δ, and μ are the g-factor, out-of-plane magnetic field, gap magnitude, and chemical potential, respectively. The g-factor of Bi is known to be $\sim$200 [38], and μ in Pb(111)/20BL-Bi(111) is estimated to be $\sim$50 meV from an extrapolation of the Bi-derived holelike bands in Fig. 4(f). Putting these values into the above equation, we obtain the minimal H_z to be 8 T, which is much larger than the upper critical field of Pb ($\sim$0.15 T) [49]. Thus, it is necessary to situate the Kramer's point of the band structure almost exactly at E_F (i.e. $\mu \sim 0$). This points to the necessity to lift up E_F by $\sim$50 meV using electric gating or electron doping to the surface by, e.g., alkali-metal deposition.

We comment here that proximity-induced superconductivity has recently been clarified in a 1 BL Bi(111) island on top of a superconducting Nb(110) substrate [20] with STM. Comparing to this Bi/Nb system, the Pb/Bi heterostructure may have an advantage in that (i) proximitized Bi film has a larger terrace so that the band structure responsible for superconductivity can be directly measured by ARPES, and (ii) one can investigate the FS-topology dependence of the SC proximity effect (this point will be detailed later). On the other hand, the Pb/Bi system also has the disadvantage that the Majorana bound state, if it exists, is likely located at the buried interface and would not be easily accessed by STM (note that fabrication of Bi on Pb is not possible at the moment due to clusterization of Pb during Bi deposition).

It should be noted that the Pb(111)/Bi(111)/TBS hybrid has a unique characteristic for studying the SC proximity effect in strongly spin–orbit-coupled materials. Since one can dramatically alter the FS topology of Bi(111) by simply varying its thickness [see the schematics in Fig. 5(d)], this hybrid would work as a useful platform to study the interplay among the band structure (FS topology), the

proximity-induced superconductivity, and the SOC. Moreover, when the 3 BL film is proximitized with a Pb film (see Fig. B1 of Appendix B for details of the ARPES data), it may host 1D topological superconductivity characterized by the SC helical edge states of a QSH insulator [50], although the QSH insulator nature needs to be further verified by other experiments such as STM and electrical transport (note that a Bi(111) ultrathin film is also interesting in the context of 1D TSC using the hinge states of higher-order TI [51]). Direct access to such edge states by local probes and detection of the Majorana zero mode are important challenges in the experiment.

4. Conclusion

We have investigated the electronic structure of an epitaxially grown heterostructure of Pb(111)/Bi(111)/TBS by ARPES. In Bi(111)/TBS, we revealed a drastic change in the band structure as a function of the Bi film thickness d, characterized by the metallic QWS ($d = 1$–2 BL), the semiconducting-like band structure ($d = 3$ BL), and the Rashba SS ($d = 5$–20 BL). We observed proximity-induced superconductivity for a 20 BL Bi(111) film when an ultra-thin Pb(111) film is epitaxially grown on it; an isotropic pairing gap of $\sim$1 meV emerges on the Bi-derived FS at $T = 5$ K. The present result lays a foundation for studying the interplay among band structure, proximity-induced superconductivity, and SOC.

Acknowledgements

We thank K. Hori, A. Tokuyama, T. Ren, and T. Saito for their assistance in the ARPES experiments. This work was supported by Grants-in-Aid for Scientific Research on Innovative Areas "Topological Materials Science" [Japan Society for the Promotion of Science (JSPS) KAKENHI Grant Numbers JP15H05853, JP18H04227, and JP15K21717], JST-CREST (No. JPMJCR18T1), JST-PRESTO (No. JPMJPR18L7), and Grants-in-Aid for Scientific Research (JSPS KAKENHI Grant Numbers JP21H04435, JP17H01139, JP18H01821, JP18H01160, JP18H04472, and JP19H01845).

Appendix A. Comparison of the electronic structure between $d = 3$ and 4 BL Bi(111)

Figure A.1(a) shows a comparison of ARPES intensity mapping at the Fermi level (E_F) for d BL Bi(111)/$TlBiSe_2$ (TBS) between $d = 4$ and 3. One clearly recognizes a similar triangular intensity pattern for the two samples. The ARPES intensity plot along the cut in Fig. A.1(b) shows the absence of a clear E_F-crossing of bands for both samples. These similarities in the Fermi surface topology and the band dispersion suggest that both samples ($d = 4$ and 3) share a common electronic structure.

Appendix B. Band structure of Pb(111)/3BL-Bi(111)

We have succeeded in fabricating a Pb(111)/3BL Bi(111) heterostructure ($d = 3$) as well as one of $d = 20$. A side-by-side comparison of the ARPES intensity mapping at E_F for a Bi(111) film ($d = 3$ BL) on TBS before and after Pb deposition shown in Figs. A.2(a) and A.2(b), respectively, reveals that the Pb deposition produces a large triangular intensity pattern outside the relatively small Bi-derived triangular feature [Fig. A.2(b)]. The Pb deposition also causes an upward shift of the topmost valence band compared to pristine 3 BL Bi(111) [Figs. A.2(c) and A.2(d)]. We remark that the shifted topmost valence band does not seem to cross E_F, suggesting that the Bi film keeps the semiconducting-like nature even after Pb deposition. This situation may be favorable to realize a 1D TSC that utilizes the superconducting metallic edge states without disturbance from the bulk conduction.

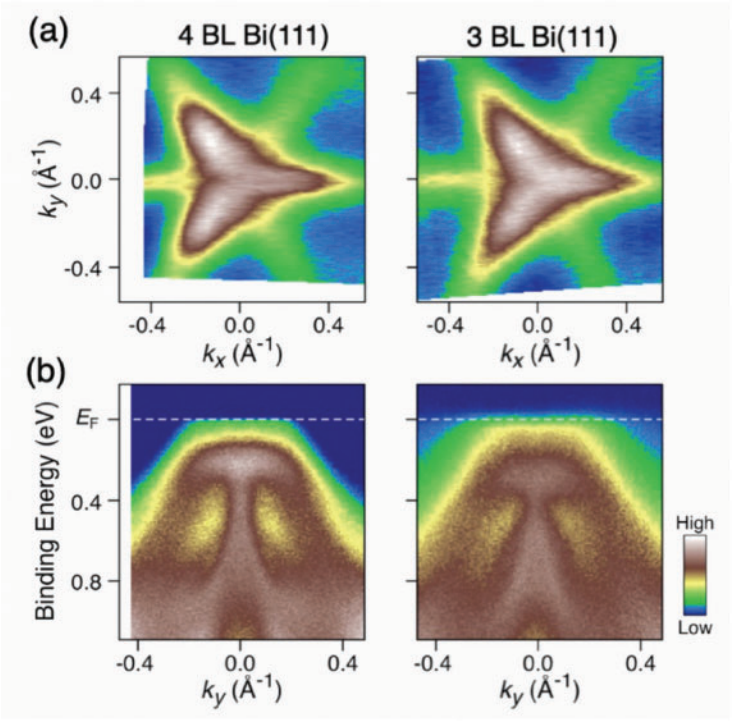

Fig. A.1. (a,b) ARPES intensity mapping at E_F and ARPES intensity plot along the $\bar{\Gamma}\bar{K}$ cut, respectively, for Bi(111) films with $d = 4$ and 3 BL, measured at $T = 30$ K with the He-Iα photons ($h\nu = 21.218$ eV).

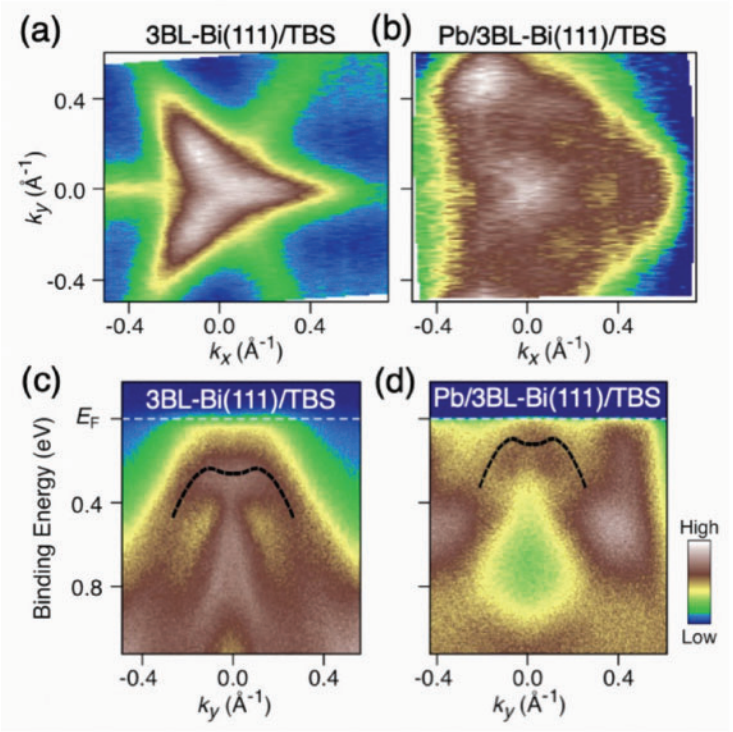

Fig. A.2. (a,b) ARPES intensity mapping at E_F for $d = 3$ BL Bi(111) film on TBS before and after Pb deposition, respectively, measured at $T = 30$ K with the He-Iα photons ($h\nu = 21.218$ eV). The Pb deposition time T_d is 13 min. (c,d) ARPES intensity plots along the $\bar{\Gamma}\bar{K}$ cut before and after Pb deposition, respectively, for the 3 BL Bi(111) film. The dashed curves are a guide for the eyes to trace the topmost valence band.

References

[1] M. Z. Hasan and C. L. Kane, Rev. Mod. Phys. **82**, 3045 (2010).
[2] X.-L. Qi and S.-C. Zhang, Rev. Mod. Phys. **83**, 1057 (2011).
[3] Y. Ando, J. Phys. Soc. Jpn. **82**, 102001 (2013).
[4] A. P. Schnyder, S. Ryu, A. Furusaki, and A. W. W. Ludwig, Phys. Rev. B **78**, 195125 (2008).
[5] M. Sato and Y. Ando, Rep. Prog. Phys. **80**, 076501 (2017).
[6] M. H. Freedman, Proc. Natl. Acad. Sci. USA **95**, 98 (1998).
[7] D. A. Ivanov, Phys. Rev. Lett. **86**, 268 (2001).
[8] A. Yu. Kitaev, Ann. Phys. **303**, 2 (2002).
[9] C. Nayak, S. H. Simon, A. Stern, M. Freedman, and S. Das Sarma, Rev. Mod. Phys. **80**, 1083 (2008).
[10] L. Fu and C. L. Kane, Phys. Rev. Lett. **100**, 096407 (2008).
[11] R. M. Lutchyn, J. D. Sau, and S. Das Sarma, Phys. Rev. Lett. **105**, 077001 (2010).
[12] Y. Oreg, G. Refael, and F. von Oppen, Phys. Rev. Lett. **105**, 177002 (2010).
[13] M. Sato and S. Fujimoto, Phys. Rev. B **79**, 094504 (2009).
[14] M.-X. Wang et al., Science **336**, 52 (2012).
[15] M. Veldhorst et al., Nat. Mater. **11**, 417 (2012).
[16] L. Maier, J. B. Oostinga, D. Knott, C. Brüne, P. Virtanen, G. Tkachov, E. M. Hankiewicz, C. Gould, H. Buhmann, and L. W. Molenkamp, Phys. Rev. Lett. **109**, 186806 (2012).
[17] S.-Y. Xu et al., Nat. Phys. **10**, 943 (2014).
[18] H.-H. Sun et al., Nano Lett. **17**, 3035 (2017).
[19] D. Flötotto, Y. Ota, Y. Bai, C. Zhang, K. Okazaki, A. Tsuzuki, T. Hashimoto J. N. Eckstein, S. Shin, and T.-C. Chiang, Sci. Adv. **4**, eaar7214 (2018).
[20] B. Jäck, Y. Xie, J. Li, S. Jeon, B. A. Bernevig, and A. Yazdani, Science **364**, 1255 (2019).
[21] V. Mourik, K. Zuo, S. M. Frolov, S. R. Plissard, E. P. A. M. Bakkers, and L. P. Kouwenhoven, Science **336**, 1003 (2012).
[22] A. Das, Y. Ronen, Y. Most, Y. Oreg, M. Heiblum, and H. Shtrikman, Nat. Phys. **8**, 887 (2012).
[23] M. T. Deng, S. Vaitiekénas, E. B. Hansen, J. Danon, M. Leijnse, K. Flensberg, J. Nygård, P. Krogstrup, and C. M. Marcus, Science **354**, 1557 (2016).
[24] S. Nadj-Perge, I. K. Drozdov, J. Li, H. Chen, S. Jeon, J. Seo, A. H. MacDonald, B. A. Bernevig, and A. Yazdani, Science **346**, 602 (2014).
[25] L. A. Wray, S.-Y. Xu, Y. Xia, Y. S. Hor, D. Qian, A. V. Fedorov, H. Lin, A. Bansil, R. J. Cava, and M. Z. Hasan, Nat. Phys. **6**, 855 (2010).
[26] C. X. Trang, Z. Wang, D. Takane, K. Nakayama, S. Souma, T. Sato, T. Takahashi, A. A. Taskin, and Y. Ando, Phys. Rev. B **93**, 241103(R) (2016).
[27] P. Zhang et al., Science **360**, 182 (2018).
[28] T. Machida, Y. Sun, S. Pyon, S. Takeda, Y. Kohsaka, T. Hanaguri, T. Sasagawa, and T. Tamegai, Nat. Mater. **18**, 811 (2019).
[29] A. Takayama, T. Sato, S. Souma, and T. Takahashi, Phys. Rev. Lett. **106**, 166401 (2011).
[30] S. Murakami, Phys. Rev. Lett. **97**, 236805 (2006).
[31] O. Prakash, A. Kumar, A. Thamizhavel, and S. Ramakrishnan, Science **355**, 52 (2017).
[32] T. Shoman, A. Takayama, T. Sato, S. Souma, T. Takahashi, T. Oguchi, K. Segawa, and Y. Ando, Nat. Commun. **6**, 6547 (2015).
[33] T. Sato, K. Segawa, H. Guo, K. Sugawara, S. Souma, T. Takahashi, and Y. Ando, Phys. Rev. Lett. **105**, 136802 (2010).
[34] C. X. Trang et al., Nat. Commun. **11**, 159 (2020).
[35] T. Hirahara, T. Nagao, I. Matsuda, G. Bihlmayer, E. V. Chulkov, Yu. M. Koroteev, P. M. Echenique, M. Saito, and S. Hasegawa, Phys. Rev. Lett. **97**, 146803 (2006).
[36] L. Miao et al., Phys. Rev. B **91**, 205414 (2015).
[37] K. Yamada, S. Souma, K. Yamauchi, N. Shimamura, K. Sugawara, C. X. Trang, T. Oguchi, K. Ueno, T. Takahashi, and T. Sato, Nano Lett. **18**, 3235 (2018).
[38] N. Shimamura et al., ACS Nano **12**, 10977 (2018).
[39] Yu. M. Koroteev, G. Bihlmayer, E. V. Chulkov, and S. Blügel, Phys. Rev. B **77**, 045428 (2008).
[40] I. K. Drozdov, A. Alexandradinata, S. Jeon, S. Nadj-Perge, H. Ji, R. J. Cava, B. A. Bernevig, and A. Yazdani, Nat. Phys. **10**, 664 (2014).
[41] W. P. Davey, Phys. Rev. **25**, 753 (1925).

[42] H. B. Michaelson, Appl. Phys. **48**, 4729 (1977).
[43] M. R. Norman et al., Nature **392**, 157 (1998).
[44] R. C. Dynes, V. Narayanamurti, and J. P. Garno, Phys. Rev. Lett. **41**, 1509 (1978).
[45] A. Chainani, T. Yokoya, T. Kiss, and S. Shin, Phys. Rev. Lett. **85**, 1966 (2000).
[46] P. A. Frigeri, D. F. Agterberg, A. Koga, and M. Sigrist, Phys. Rev. Lett. **92**, 097001 (2004); **93**, 099903 (2004) [erratum].
[47] A. V. Matetskiy, S. Ichinokura, L. V. Bondarenko, A. Y. Tupchaya, D. V. Gruznev, A. V. Zotov, A. A. Saranin, R. Hobara, A. Takayama, and S. Hasegawa, Phys. Rev. Lett. **115**, 147003 (2015).
[48] Y. Nakata, K. Sugawara, S. Ichinokura, Y. Okada, T. Hitosugi, T. Koretsune, K. Ueno, S. Hasegawa, T. Takahashi, and T. Sato, npj 2D Mater. Appl. **2**, 12 (2018).
[49] T. Zhang et al., Nat. Phys. **6**, 104 (2010).
[50] S. Hart, H. Ren, T. Wagner, P. Leubner, M. Mühlbauer, C. Brüne, H. Buhmann, L. W. Molenkamp, and A. Yacoby, Nat. Phys. **10**, 638 (2014).
[51] F. Schindler, A. M. Cook, M. G. Vergniory, Z. Wang, St. S. P. Parkin, B. A. Bernevig, and T. Neupert, Sci. Adv. **4**, eaat0346 (2018).